Contribution from the Departments of Chemistry, The Chung Cheng Institute of Technology, Taiwan, Republic of China, and The University of Mississippi, University, Mississippi 38677

Lower Valence Fluorides of Vanadium. 7. Dependence of Structure and Magnetic Properties of the Modified Pyrochlores Rb_xVF_3 and Cs_xVF_3 on Composition

Y. S. HONG,[1a] R. F. WILLIAMSON,[1b] and W. O. J. BOO*[1b]

Received December 8, 1981

The modified pyrochlores Rb_xVF_3 and Cs_xVF_3 exist over the composition range $x = 0.45$–0.52. Optical and magnetic analyses provide evidence of two distinct crystal structures (cubic and orthorhombic) within each system. X-ray studies confirm the existence of both structures in Cs_xVF_3 but only orthorhombic in Rb_xVF_3. At small x, both structures coexist; at large x, only the orthorhombic phase is present. The orthorhombic phase is believed to be an ionically (electronically) ordered structure consisting of linear chains of V^{2+} ions that are orthogonal to linear chains of V^{3+} ions. This ordering distorts the dimensions of the ortho-cubic unit cell from being exactly $2^{1/2}|a| = 2^{1/2}|b| = |c|$. The orthorhombic unit cell dimensions of $Rb_{0.50}VF_3$ are $a = 7.463$, $b = 7.249$, and $c = 10.185$ Å, those of $Cs_{0.50}VF_3$ are $a = 7.472$, $b = 7.441$, and $c = 10.435$ Å, and the cubic dimension of $Cs_{0.50}VF_3$ is $a = 10.491$ Å. Magnetic ordering (T_N) in Cs_xVF_3 occurs at 11 K independent of composition, but in Rb_xVF_3 it varies from 10 to 5 K as x increases. Curie constants (C_M) indicate the orbital moment of V^{3+} is partially quenched in the cubic phase but totally quenched in the orthorhombic. Curie–Weiss constants (Θ) range from −3 to −23 K in Rb_xVF_3 and from +4 to −3 K in Cs_xVF_3, indicating the presence of both antiferromagnetic and ferromagnetic exchange interactions. The origins of these two types of interactions are speculated to be delocalization and correlation, respectively. Small induced magnetic moments associated with the cubic phase are interpreted as a measure of V^{2+}–V^{3+} disorder in that phase.

Introduction

In the two previous papers of this series, ionic (electronic) and magnetic orderings were reported for the tetragonal system K_xVF_3[2a] ($x = 0.45$–0.56) and the pseudohexagonal systems A_xVF_3[2b] ($x \approx 0.2$–0.3 and A = K, Rb, Tl, Cs). In these systems the consequences of electronic ordering are crystal distortions, modulated structures, and a variety of domain structures. In the tetragonal system, magnetic ordering and subsequent quantitative magnetic moments further reflected the electronic ordering. In the pseudohexagonal systems, magnetic moments resulting from magnetic order revealed that electronic ordering in these systems occurs cooperatively with ionic ordering of A^+ ions in partially filled sites.

This paper reports electronic and magnetic ordering found in the modified pyrochlore systems Rb_xVF_3 and Cs_xVF_3. Preparation of these systems was first reported by Cros et al.[3] Composition limits were reported in the ranges $x = 0.45$–0.50 for Rb_xVF_3 and 0.48–0.50 for Cs_xVF_3. At the lower value of x, both systems were reported to have cubic structures, but at $x = 0.50$, the former was reported as orthorhombic and the latter as tetragonal. No satisfactory explanation was given for these results, nor were any magnetic results reported.

Experimental Results

Preparation of the Rb_xVF_3 and Cs_xVF_3 modified pyrochlores consisted of five samples for each system with $x = 0.45$, 0.475, 0.50, 0.525, and 0.55. The method of preparation utilizing vacuum encapsulation in molybdenum and characterization by optical microscopy, X-ray diffraction (Guinier–Hägg), and magnetic measurements (PAR vibrating-sample magnetometer) were described previously.[2] A low temperature of 2.4 K was obtained by pumping on liquid helium. Chemical analyses were done by Galbraith, and these too were described previously.[2]

Examination by optical microscopy revealed homogeneous, well-formed, crystalline products. The transmitted color of the modified pyrochlore phase is brownish red, and all samples were observed to be optically dense. The Rb_xVF_3 samples, upon examination by polarized microscopy, were found to be moderately birefringent at $x \geq 0.50$, becoming almost isotropic at $x < 0.50$. The Cs_xVF_3 samples ranged from weakly birefringent, $x \geq 0.50$, to isotropic for $x < 0.50$. The principal impurity phases in Rb_xVF_3 were VF_2 (blue, highly birefringent) and $RbVF_3$ (pale blue, isotropic); in Cs_xVF_3, only VF_2 was observed. These blue crystals were removed from the samples by Pasteur's method prior to chemical analyses and X-ray and magnetic measurements. Chemical analyses are shown in Table I.

Table I. Chemical Analyses

sample designation	element	% calcd	% found	formula exptl	formula theor
$Rb_{0.45}VF_3$	Rb	26.27	26.09	$Rb_{0.451}VF_{3.01}$	$Rb_{0.45}VF_3$
	V	34.80	34.45		
	F	38.93	38.73		
$Rb_{0.475}VF_3$	Rb	27.33	26.96	$Rb_{0.465}VF_{2.98}$	$Rb_{0.475}VF_3$
	V	34.30	34.53		
	F	38.37	38.42		
$Rb_{0.50}VF_3$	Rb	28.36	27.95	$Rb_{0.492}VF_{3.03}$	$Rb_{0.50}VF_3$
	V	33.81	33.84		
	F	37.83	38.27		
$Rb_{0.525}VF_3$	Rb	29.36	29.37	$Rb_{0.523}VF_{2.99}$	$Rb_{0.525}VF_3$
	V	33.34	33.46		
	F	37.30	37.28		
$Cs_{0.45}VF_3$	Cs	35.65	33.88	$Cs_{0.446}VF_{3.18}$	$Cs_{0.45}VF_3$
	V	30.37	29.10		
	F	33.98	34.54		
$Cs_{0.475}VF_3$	Cs	36.90	33.64	$Cs_{0.402}VF_{2.48}$	$Cs_{0.475}VF_3$
	V	29.78	32.05		
	F	33.32	29.62		
$Cs_{0.50}VF_3$	Cs	38.11	37.81	$Cs_{0.497}VF_{3.02}$	$Cs_{0.50}VF_3$
	V	29.21	29.17		
	F	32.68	32.89		
$Cs_{0.525}VF_3$	Cs	39.26	38.94	$Cs_{0.523}VF_{3.01}$	$Cs_{0.525}VF_3$
	V	28.67	28.55		
	F	32.07	32.00		
$Cs_{0.55}VF_3$	Cs	40.38	38.68	$Cs_{0.510}VF_{2.96}$	$Cs_{0.55}VF_3$
	V	28.14	29.07		
	F	31.48	32.11		

No significant differences were found between Guinier–Hägg films of Rb_xVF_3. The Cs_xVF_3 X-ray results, however, indicated subtle composition-dependent differences. It is apparent from the optical analysis that both systems are almost cubic. It is also readily seen from the X-ray data that both systems are distorted slightly from cubic. All reflections from each Rb_xVF_3 film were indexed to orthorhombic unit cells of dimensions 7.5 × 7.2 × 10.2 Å, but no cubic modified py-

(1) (a) The Chung Cheng Institute of Technology. (b) The University of Mississippi.
(2) (a) Y. S. Hong, R. F. Wiliamson, and W. O. J. Boo, *Inorg. Chem.*, **19**, 2229 (1980). (b) Y. S. Hong, R. F. Williamson, and W. O. J. Boo, *ibid.*, **20**, 403 (1981).
(3) C. Cros, R. Feurer, M. Pouchard, and P. Hagenmuller, *Mater. Res. Bull.*, **10**, 383 (1975).

0020-1669/82/1321-3898$01.25/0

rochlore phase was observed. Guinier–Hägg results of $Rb_{0.50}VF_3$ with Cr $K\alpha_1$ radiation are shown in Table II (supplementary material). X-ray diffraction results of the Cs_xVF_3 system are shown in Table III (supplementary material). Here, too, all reflections from each sample were fitted to orthorhombic unit cells of dimensions 7.5 × 7.4 × 10.4 Å. Unlike the Rb_xVF_3 system, these dimensions change slightly with x, and in addition to an orthorhombic characterization, selected reflections were also indexed to a cubic unit cell ($a \approx 10.5$ Å). At low x, the fit to both systems is excellent, but at $x > 0.50$ the cubic correlation becomes poor. The intensities also corroborate this fitting to both orthorhombic and cubic unit cells. In samples $Cs_{0.45}VF_3$, $Cs_{0.475}VF_3$ and $Cs_{0.50}VF_3$ the intensities of the cubic lines are of greater intensity than their counterparts in samples $Cs_{0.525}VF_3$ and $Cs_{0.55}VF_3$.

It is obvious that the orthorhombic unit cells result as distortions from cubic symmetry. A face-centered cubic lattice can be described by a set of tetragonal base vectors whose unit cell has half the volume of the cubic unit cell but is body centered. It is this unit cell that upon distortion becomes orthorhombic; hence, we shall refer to it as the ortho-cubic unit cell. The undistorted ortho-cubic unit cell has dimensions $|a_o| = |a_c|/2^{1/2}$, $|b_o| = |a_c|/2^{1/2}$, and $|c_o| = |a_c|$. If the orthorhombic vectors are chosen such that $a_o = {}^1/_2a_c - {}^1/_2b_c + 0$, $b_o = {}^1/_2a_c + {}^1/_2b_c + 0$, and $c_o = 0 + 0 + c_c$, the matrix for transforming cubic Miller indices into orthorhombic ones is

$$\begin{pmatrix} {}^1/_2 & \overline{{}^1/_2} & 0 \\ {}^1/_2 & {}^1/_2 & 0 \\ 0 & 0 & 1 \end{pmatrix}$$

Observable reflections from the cubic phase should be *hkl* all even or all odd, and from the orthorhombic phase the sum of h, k, and l should be an even integer ($h + k + l = 2n$). A cubic (*hkl*) reflection permuted in all possible ways (i.e., 48), including positive and negative signs, will in general be transformed into six families of ortho-cubic reflections. If the ortho-cubic unit cell is distorted to true orthorhombic, six unique reflections of approximately equal intensities may be observed on a random powder X-ray diffraction photograph. Special reflections such as cubic (*hhh*) will give rise to only two observable orthorhombic reflections with approximate relative intensities 1:1. Furthermore, cubic (*hhl*), (*hh*0), (*kk*0), and (*h*00) reflections may be split into four, three, four, and two orthorhombic reflections with approximate relative intensities 1:1:2:2, 1:1:4, 1:1:2:2, and 1:2, respectively. In Tables II and III, the orthorhombic Miller indices are grouped beside the face-centered cubic reflections of their origin. The number and relative intensities of these reflections are consistent with the rules predicted above. In the Cs_xVF_3 system (Table III) every orthorhombic reflection from every sample fits this pattern. In Rb_xVF_3, however (Table II), many additional orthorhombic reflections do not fit this scheme. Instead, the rubidium data describe a primitive orthorhombic lattice. A summary of Guinier–Hägg results with Cr $K\alpha_1$ and Cu $K\alpha_1$ radiation for the Rb_xVF_3 and Cs_xVF_3 systems is given in Table IV. In addition to lattice constants, distortion ratios are shown to give a qualitative indication of the distortion of the ortho-cubic unit cell. These ratios are defined as

$$\frac{2^{1/2}|a|}{10.49} : \frac{2^{1/2}|b|}{10.49} : \frac{|c|}{10.49}$$

These distortion ratios compare a, b, and c of the orthorhombic unit cell with a (10.49 Å) of cubic Cs_xVF_3.

Magnetic susceptibility measurements were made on each sample from 4.2 to 300 K at 10 kG. Plots of χ^{-1} vs. T for Rb_xVF_3 and Cs_xVF_3 are shown in Figures 1 and 2. In both systems there exists a linear paramagnetic region above ~30 K. The Rb_xVF_3 plots do not give indication of a specific ordering temperature, but those of Cs_xVF_3 consistently show an upward break in slope at 11 K. So that long-range magnetic ordering temperatures could be definitely established, isothermal measurements were made at 2.4, 4.2, 5, 6, 7, 8, 9, 10, and 11 K. At each temperature, magnetic moments were

Table IV. Summary of Lattice Constants (±0.05%, Å) of Modified Pyrochlores Rb_xVF_3 and Cs_xVF_3

	Cu data			Cr data		
sample designation	orthorhombic[a]	cubic	distortion ratios	orthorhombic[a]	cubic	distortion ratios
$Rb_{0.45}VF_3$	7.464		1.006	7.458		1.005
	7.249		0.977	7.246		0.977
	10.187		0.971	10.186		0.971
$Rb_{0.475}VF_3$	7.463		1.006	7.461		1.006
	7.250		0.977	7.248		0.977
	10.189		0.971	10.186		0.971
$Rb_{0.50}VF_3$	7.464		1.006	7.463		1.006
	7.252		0.978	7.249		0.977
	10.186		0.971	10.185		0.971
$Rb_{0.525}VF_3$	7.467		1.007	7.466		1.006
	7.254		0.978	7.251		0.977
	10.190		0.971	10.194		0.972
$Rb_{0.55}VF_3$	7.467		1.007	7.463		1.006
	7.255		0.978	7.251		0.977
	10.189		0.971	10.186		0.971
$Cs_{0.45}VF_3$	7.468	10.492	1.007	7.468	10.494	1.007
	7.438		1.003	7.438		1.003
	10.449		0.996	10.449		0.996
$Cs_{0.475}VF_3$	7.467	10.490	1.007	7.460	10.491	1.006
	7.441		1.003	7.435		1.002
	10.449		0.996	10.449		0.996
$Cs_{0.50}VF_3$	7.474	10.491	1.008	7.472	10.491	1.007
	7.445		1.004	7.441		1.003
	10.442		0.995	10.435		0.995
$Cs_{0.525}VF_3$	7.491		1.010	7.485		1.009
	7.445		1.004	7.441		1.003
	10.435		0.995	10.429		0.994
$Cs_{0.55}VF_3$	7.488		1.009	7.484		1.009
	7.447		1.004	7.440		1.003
	10.436		0.995	10.426		0.994

[a] The three values given for each sample are the orthorhombic unit cell dimensions a, b, and c, respectively.

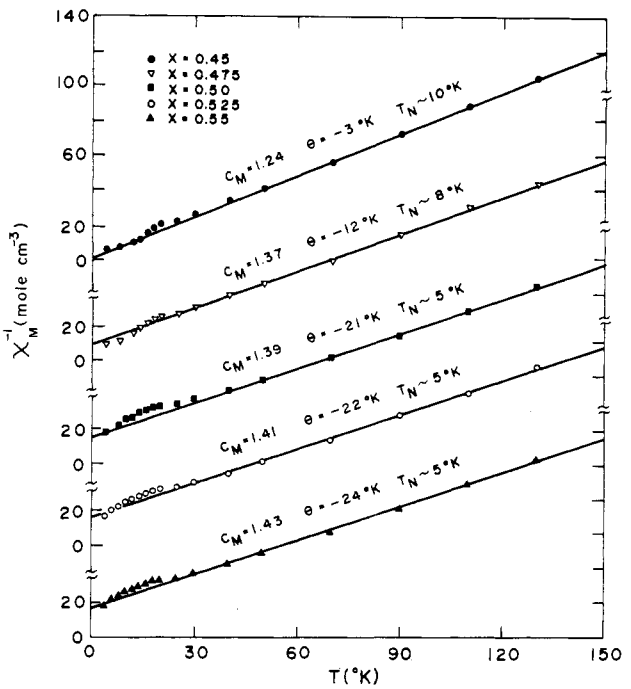

Figure 1. Inverse magnetic susceptibilities vs. temperature at 10 kG for Rb_xVF_3.

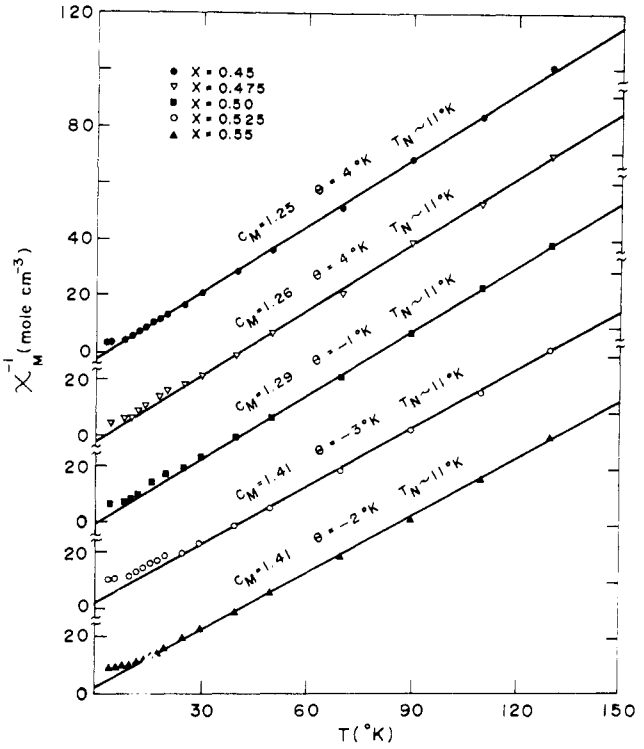

Figure 2. Inverse magnetic susceptibilities vs. temperature at 10 kG for Cs_xVF_3.

Table V. Summary of Magnetic Constants of the Rb_xVF_3 and Cs_xVF_3 Modified Pyrochlore Systems

sample designation	C_M, cm^3 deg mol^{-1} obsd	calcd partially quenched	calcd totally quenched	Θ, K	T_N, K	σ_0, μ_B
$Rb_{0.45}VF_3$	1.24	1.24	1.35	−3	10	0.05
$Rb_{0.475}VF_3$	1.37	1.26	1.37	−12	8	0.05
$Rb_{0.50}VF_3$	1.39	1.29	1.40	−21	5	0.03
$Rb_{0.525}VF_3$	1.41	1.32	1.42	−22	5	0.03
$Rb_{0.55}VF_3$	1.43	1.34	1.44	−24	5	0.05
$Cs_{0.45}VF_3$	1.25	1.24	1.35	4	11	0.13
$Cs_{0.475}VF_3$	1.26	1.26	1.37	4	11	0.12
$Cs_{0.50}VF_3$	1.29	1.29	1.40	1	11	0.07
$Cs_{0.525}VF_3$	1.41	1.32	1.42	−3	11	0.03
$Cs_{0.55}VF_3$	1.41	1.34	1.44	−2	11	0.02

measured at fields of 10, 9, 8, 7, 6, 5, 4, 3, 2, 1, and 0 kG. Values of the moments plotted vs. field were found to be linear in the region 5–10 kG. Spontaneous moments (σ) at each temperature were obtained by extrapolating values from these linear regions to zero field. The zero-field (spontaneous) moments per molar formula unit of Rb_xVF_3 and Cs_xVF_3 are plotted vs. temperature in Figures 3 and 4, respectively. The smooth curves drawn on these plots are extrapolated to 0 K to give σ_0 values reported in Table V. The temperature at which σ goes to zero is the temperature where three-dimensional long-range ordering sets in and is reported in Table V as T_N. In the case of Cs_xVF_3, values for T_N obtained from the plots of σ vs. T in Figure 4 are identical with those obtained from plots of χ^{-1} vs. T in Figure 2. For Rb_xVF_3, however, values of T_N shown in Figure 3 range from 10 to 5 K.

Discussion

The chemical analyses indicate that both Rb_xVF_3 and Cs_xVF_3 modified pyrochlore phases exist within the composition range x = 0.45–0.52. Optical analyses by polarized microscopy indicate the existence of two phases in each system. At small x there is evidence of a cubic phase, but at large x

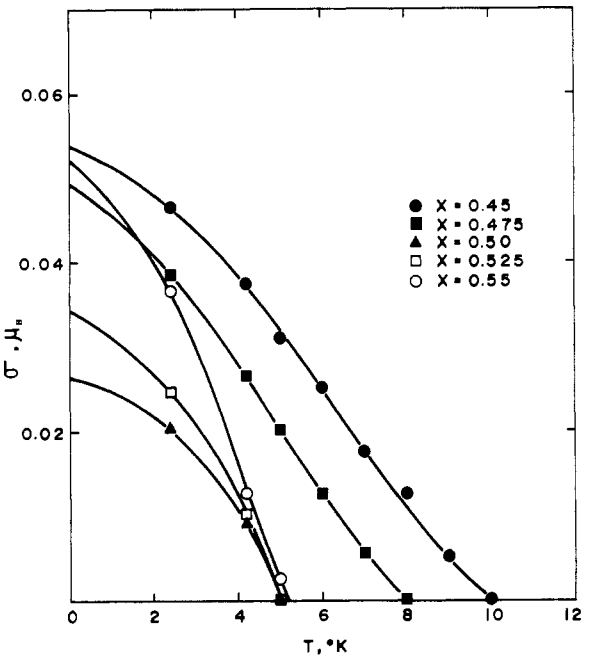

Figure 3. Spontaneous magnetic moments of Rb_xVF_3 vs. temperature for samples cooled in a 10-kG field.

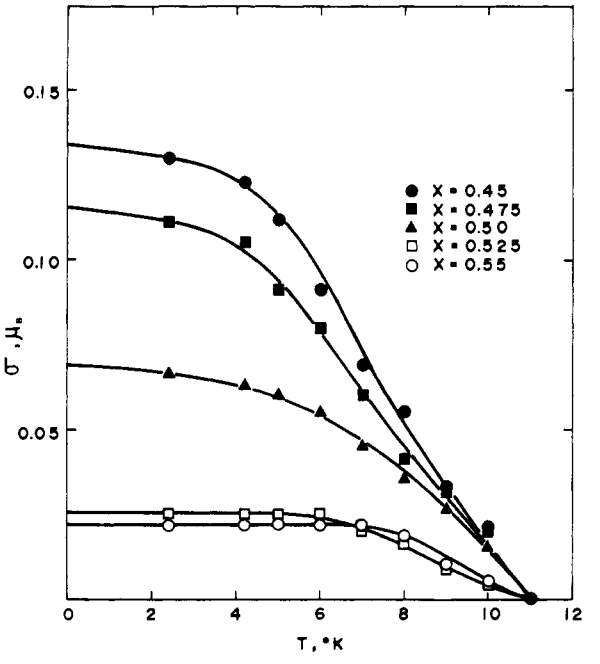

Figure 4. Spontaneous magnetic moments of Cs_xVF_3 vs. temperature for samples cooled in a 10-kG field.

the structure is of lower symmetry. Guinier–Hägg X-ray results were less certain regarding the existence of the cubic phase. In the Rb_xVF_3 system, all reflections in each sample were indexed to an orthorhombic unit cell, and no fit to a cubic unit cell was found. In the Cs_xVF_3 system, all reflections in each sample were indexed to an orthorhombic unit cell; however, for x = 0.45 and 0.475, selected lines could be indexed to a cubic unit cell as well. At x = 0.50, the cubic fit was not as good, and for x = 0.525 and 0.55, the cubic fit became poor. The most likely explanation for these results is the existence of defect structures involving intergrowth of the cubic and orthorhombic phases. The extent to which the ortho-cubic unit cell is distorted is demonstrated semiquantitatively by the distortion ratios in Table IV. One sees immediately that distortion of Cs_xVF_3 is small and is distributed approximately evenly over a, b, and c. In Rb_xVF_3, however, the distortion,

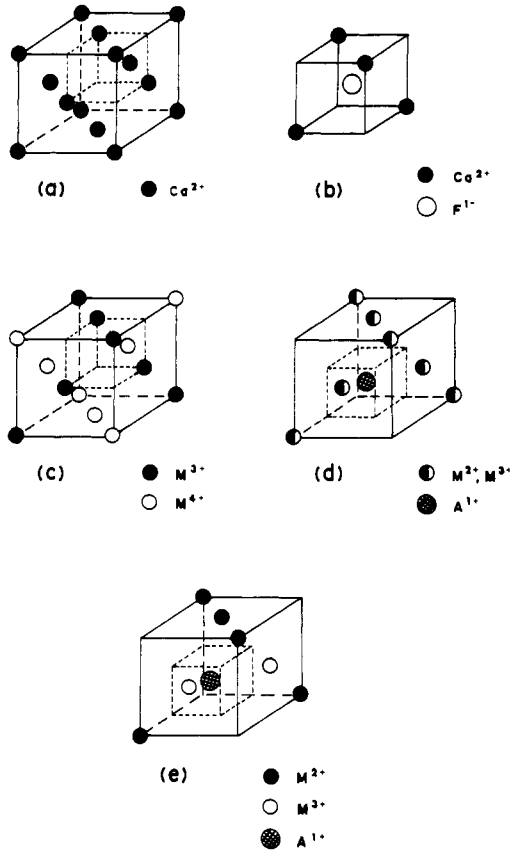

Figure 5. (a) The CaF_2 unit cell, showing only the Ca^{2+} ions. (b) One of the eight tetrahedral holes of CaF_2 occupied by the F^- ion. (c) One-eighth of the pyrochlore unit cell, $M^{III}_2M^{IV}_2O_7$, showing ionic ordering of M^{3+} and M^{4+}. (d) One-eighth of the unit cell of modified pyrochlore, $A^IM^{II}M^{III}F_6$, showing random locations of M^{2+} and M^{3+} and the location of A^+. (e) One-eighth of the unit cell of the ionically ordered modified pyrochlore structure.

which is much greater, is primarily a collapse of b and c. It is obvious that the magnitude of the distortion in Rb_xVF_3 would make intergrowth with a cubic phase unfavorable. In Cs_xVF_3 the distortion ratios increase slightly with increasing x, suggesting that intergrowth of the orthorhombic phase with the cubic phase is more likely to occur at low x.

The reason the modified pyrochlore phase distorts to orthorhombic symmetry has never been satisfactorily answered. It has been observed that the orthorhombic phase occurs only for homonuclear systems[3-5] (i.e., when M^{II} and M^{III} are the same element). This fact suggests very strongly that electronic ordering can occur in the modified pyrochlore phase, but mechanisms for ionic M^{2+}–M^{3+} ordering (when M^{II} and M^{III} are different elements) are less favorable.

Close analogies can be drawn between the orthorhombic phase of the modified pyrochlore system Rb_xVF_3 and the weberite structure. The weberite compound Na_2NiFeF_7,[6] for example, has lattice dimensions a = 7.45, b = 7.23, and c = 10.34 Å, which compare favorably with those of $Rb_{0.50}VF_3$: a = 7.46, b = 7.25, and c = 10.19 Å. In the weberite structure, the M^{2+} ions form a network of ordered linear chains that lie parallel to the crystallographic a axis. The M^{3+} ions, however, have only M^{2+} ions for nearest neighbors, so further analogies between weberite and the modified pyrochlore must be approached with caution.

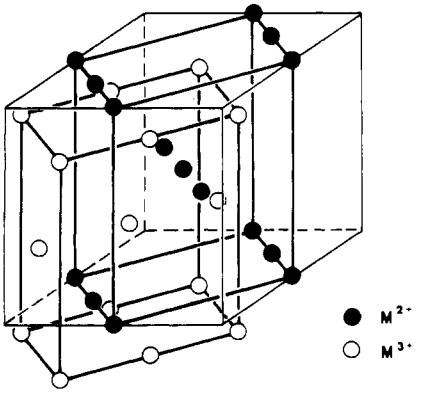

Figure 6. Proposed ionically ordered structure of the modified pyrochlore, showing the interpenetrating orthrohombic unit cells.

To understand the possibility of electronic ordering in the modified pyrochlore structure, we should first make analogies to the fluorite and the pyrochlore structures. The fluorite structure (CaF_2) is illustrated in Figure 5a,b. In this unit cell (Figure 5a) the Ca^{2+} ions lie on fccub equivalent positions. Figure 5b shows one of eight tetrahedral holes which are occupied by F^- ions. The pyrochlore structure has a unit cell 8 times that of fluorite. For oxides of the general formula $M^{III}_2M^{IV}_2O_7$ having the pyrochlore structure,[7-9] nearest-neighboring M^{3+} ions form ordered linear chains in the six face diagonal directions. The M^{4+} ions do likewise in the same six directions, allowing the structure to be ionically ordered while retaining cubic symmetry. One-eighth of a unit cell of pyrochlore is shown in Figure 5c. In this figure only M^{3+} and M^{4+} ions are shown. In pyrochlore, seven of the eight tetrahedral holes are occupied by O^{2-} ions. The tetrahedral hole with four M^{3+} ions at its corners (shown in Figure 5c) is empty. The pyrochlore unit cell is made up of four cubes similar to the one shown in Figure 5c and four others that are inverted images of it. These eight cubes packed in an alternating (or NaCl) type arrangement make up the cubic unit cell.

The modified pyrochlore structure found for fluorides ($A^IM^{II}M^{III}F_6$)[10-12] is reported to have only half as many multivalent cations per unit cell as the pyrochlore structure. Sites that were previously identified as tetrahedral holes in pyrochlore no longer have multivalent cations on all four tetrahedral corners. One-eighth of the modified pyrochlore structure is illustrated in Figure 5d. In this figure, M^{2+} and M^{3+} ions are randomly arranged. Only one of eight previous tetrahedral holes is intact with four cations on tetrahedral corners. Six holes that were previously tetrahedral now have only two tetrahedral corners occupied, and one site that was formerly a tetrahedral hole no longer has any occupied corners. That site is illustrated in Figure 5d and is occupied by the A^+ cation. The six former tetrahedral holes with half of the corners occupied are filled with F^- ions, and the only true tetrahedral hole with four corners occupied is empty. In the cubic modified pyrochlore structure, randomly oriented M^{2+}–M^{3+} ions form an infinite –M–F–M–F–M– network in six face diagonal directions. These M^{2+}–M^{3+} cations are located on sites previously occupied by only M^{3+} (or M^{4+}) in pyrochlore.

(4) A. Tressaud, R. de Pape, and J. Portier, *C. R. Hebd. Seances Acad. Sci.*, **270**, 726 (1970).
(5) D. Dumora, J. Ravez, and P. Hagenmuller, *J. Solid State Chem.*, **5**, 35 (1972).
(6) G. Heger, *Int. J. Magn.*, **5**, 119 (1973).
(7) F. Jona, G. Shirane, and R. Pepinsky, *Phys. Rev.*, **98**, 903 (1955).
(8) J. M. Longo, P. M. Raccah, and J. B. Goodenough, *Mater. Res. Bull.*, **4**, 191 (1969).
(9) J. Pannetier and J. Lucas, *Mater. Res. Bull.*, **5**, 797 (1970).
(10) E. Banks, O. Berkooz, and J. A. De Luca, *Mater. Res. Bull.*, **6**, 659 (1971).
(11) E. Banks, J. A. De Luca, and O. Berkooz, *J. Solid State Chem.*, **6**, 569 (1973).
(12) D. Babel, G. Pausewang, and W. Viebahn, *Z. Naturforsch., B: Anorg. Chem., Org. Chem., Biochem., Biphys., Biol.*, **22B**, 1219 (1967).

The proposed electronically ordered modified pyrochlore structure is illustrated in Figure 5e. As stated previously, only homonuclear systems have been reported to distort the cubic unit cell to orthorhombic. If M^{2+} ions form ordered linear chains in one of the six directions, then M^{3+} ions will necessarily do the same in a second direction. The other four directions will consist of alternate M^{2+}–M^{3+} order. This ionic order should distort the cubic unit cell to orthorhombic with pseudotetragonal dimensions $|a| \approx |b| \approx |c|/2^{1/2}$. Furthermore, the modified pyrochlore structure is face-centered cubic, and the orthorhombic structure resulting from rotation of a and b by 45° should be body centered. This proposed ordered structure is illustrated in Figure 6. The orthorhombric unit cell can be represented by either M^{2+} ions or M^{3+} ions occupying lattice positions. Both of these representations, and how they interpenetrate, are shown in the figure. The two unit cell representations can be brought into approximate coincidence by rotating one of them by 90° and translating it one-fourth of the vector distances along each of the orthorhombic a, b, and c axes. This operation allows only approximate coincidence because of the distortion of the ortho-cubic unit cell.

The X-ray data of the Cs_xVF_3 system (Table III) fit the model shown in Figure 6. The cubic phase is face centered, and the orthorhombic phase is body centered. No forbidden reflections were observed. The Rb_xVF_3 system, however (Table II), is obviously not a perfect body-centered structure as evidenced by numerous weak reflections of which $h + k + l = 2n + 1$. It is apparent from observation of the orthorhombic lattice dimensions of Rb_xVF_3 and Cs_xVF_3 that the parent lattice collapses around the smaller Rb^+ ion in the b and c directions, further reducing the symmetry of Rb_xVF_3. Not only do Rb_xVF_3 and Cs_xVF_3 belong to different space groups, but they also have different Bravais lattices; one is primitive and the other is body centered. Further comparison with weberite can now be made. The proposed ionically ordered modified pyrochlore structure (shown in Figure 6) and weberite have the same ordered structure for the Mn^{2+} ion, thus explaining the similarity in lattice dimensions of Na_2NiFeF_7 and $Rb_{0.50}VF_3$. In weberite, however, the M^{3+} ions do not form ordered linear chains. It should also be pointed out that the distortion of Rb_xVF_3 from body centered to primitive cannot be explained by analogy to weberite because the latter is body centered. The analogy to weberite, however, does suggest the linear chains of M^{2+} ions lie along the a axis and chains of M^{3+} ions lie along b.

The magnetic data provide additional ionic as well as magnetic structural information. As the orthorhombic phases of Rb_xVF_3 and Cs_xVF_3 are different structures, their magnetic behavior is also different. Since the Cs_xVF_3 crystal system is well-behaved, its magnetic behavior is more easily explained.

Magnetic Behavior in Cs_xVF_3. In the Cs_xVF_3 system, the orthorhombic phase is distorted only slightly from cubic symmetry. This distortion is the combination of two effects related to the ionic order. First, the relative size of the V^{2+} ion to that of V^{3+} would cause an expansion along the direction of ordered rows of V^{2+} ions and contraction along rows of V^{3+} ions. Second, the V^{3+} ions have the greater charge, and therefore, repulsion between V^{3+} ions would cause rows of V^{3+} ions to expand relative to rows of V^{2+} ions. These two effects nearly cancel each other in the Cs_xVF_3 case. The small distortion is a consequence of simple expansion or contraction in the orthorhombic a and b directions, so the orthorhombic unit cell remains body centered.

The Curie constants are useful in determining whether the orbital moment of the V^{3+} ion is partially or totally quenched. In the preceding paper[2b] it was seen that C_M is the sum of contributions from V^{2+} and V^{3+}:

$$C_M = xC_{2+} + (1 - x)C_{3+}$$

For V^{2+}

$$C_{2+} = \frac{Ng_{2+}^2\mu_B^2(3/2)(3/2 + 1)}{3k}$$

and for V^{3+}

$$C_{3+} = \frac{Ng_{3+}^2\mu_B^2(1)(1 + 1)}{3k}$$

where N is Avogadro's number, g_{2+} and g_{3+} are the Landé splitting factors for V^{2+} and V^{3+}, respectively, μ_B is the Bohr magneton, and k is Boltzmann's constant. The value of g_{2+} found to be 1.97 in the paramagnetic regions of VF_2[13] and KVF_3[14] and the average value of 1.74 for g_{3+} from the paramagnetic region of VF_3[15] fit the pseudohexagonal A_xVF_3 systems[2b] very well. In these structures, the orbital contribution to the magnetic susceptibility of V^{3+} is only partially quenched. If the orbital moment of V^{3+} is totally quenched, then g_{3+} would be approximately 2.00. Measured C_M values indicate that this is the case in the tetragonal K_xVF_3 phase.[2a] In Table V, experimental values of C_M for the modified pyrochlore phase Cs_xVF_3 are compared with two sets of theoretical values. For the case in which the orbital moment of V^{3+} is partially quenched, C_M values were calculated from $g_{2+} = 1.97$ and $g_{3+} = 1.74$. For totally quenched moments, the values $g_{2+} = g_{3+} = 1.97$ were used. The C_M values indicate V^{3+} orbital moments are partially quenched in $Cs_{0.45}VF_3$, $Cs_{0.475}VF_3$, and $Cs_{0.50}VF_3$ and totally quenched in $Cs_{0.525}VF$ and $Cs_{0.55}VF_3$. Apparently, ionic ordering is sufficient to distort the VF_6^{3-} octahedra, and the orbital moment of V^{3+}, which is only partially quenched in the cubic phase, becomes totally quenched in the orthorhombic phase.

The Curie–Weiss constants, Θ, of Cs_xVF_3 are very close to 0 K, which means both ferromagnetic and antiferromagnetic interactions are present and are of approximately the same magnitude overall. This is somewhat surprising as V–F–V interactions in the modified pyrochlore structure are close to 180°, and all V–V interactions of this kind studied previously were found to be antiferromagnetic. It was learned from VF_3[15] that a V^{3+}–F–V^{3+} 180° interaction is weakly antiferromagnetic, from the tetragonal K_xVF_3 system[2a] that the 180° V^{2+}–F–V^{3+} interaction is weak to moderate antiferromagnetic, and from KVF_3[14] that the 180° V^{2+}–F–V^{2+} interaction is moderately antiferromagnetic. All of the experimental evidence for these three cases can be explained by the Goodenough–Kanamori rules,[16,17] which employ the correlation model for superexchange. One explanation for the ferromagnetic behavior implied by Θ values in Cs_xVF_3 is the exchange mechanism involves delocalization as well as correlation. The electronic configurations of V^{2+} (d^3) and V^{3+} (d^2) in an octahedral crystal field, with V ions located at the corners of tetrahedra, produce an arrangement of empty and half-filled t_{2g} orbitals conducive to delocalization. According to Goodenough,[16] a delocalization magnetic exchange between half-filled and empty orbitals will lead to a ferromagnetic interaction.

The values of T_N were established from plots of χ^{-1} vs. T and plots of σ vs. T to be 11 K over the entire composition range. The reason for this consistency is there is little structural difference between the orthorhombic and cubic phases in Cs_xVF_3 (the distortion ratios indicate the distortion to be about 0.5%).

(13) J. W. Stout and H. Y. Lau, *J. Appl. Phys.*, **38**, 1472 (1967).
(14) R. F. Williamson and W. O. J. Boo, *Inorg. Chem.*, **16**, 646 (1977).
(15) A. C. Gossard, H. J. Guggenheim, F. S. L. Hsu, and R. C. Sherwood, *AIP Conf. Proc.*, **No. 5**, 302 (1971).
(16) J. B. Goodenough, "Magnetism and the Chemical Bond", Interscience, New York, 1963, pp 165–185.
(17) J. Kanamori, *J. Phys. Chem. Solids*, **10**, 87 (1959).

Finally, the spontaneous moments seem to be associated with the cubic phase. These moments are actually induced moments that disappear when the external magnetic field is removed. The small moments observed in samples of $Cs_{0.525}VF_3$ and $Cs_{0.55}VF_3$ are probably a measure of crystal defects in those phases.

Magnetic Behavior in Rb_xVF_3. The distortion of the orthorhombic phase from cubic symmetry is much larger in Rb_xVF_3 than in Cs_xVF_3, although its origin is the same—namely, from ionic ordering. This distortion in Rb_xVF_3 is not simple as in Cs_xVF_3 but involves moving V and probably F to positions of lower symmetry. This change in the packing structure is reflected in the magnetic properties of Rb_xVF_3.

As in Cs_xVF_3, the values of C_M indicate V^{3+} orbital moments are partially quenched in the cubic phase and totally quenched in the orthorhombic phase of Rb_xVF_3. The Θ values in Rb_xVF_3 change significantly with composition. In $Rb_{0.45}VF_3$ a considerable amount of the cubic phase is present. As in Cs_xVF_3, delocalization in cubic Rb_xVF_3 makes a contribution to the magnetic interactions that all but cancels the antiferromagnetic contribution made by correlation effects. In the orthorhombic phase of Rb_xVF_3, however, distortion of the V and F ions significantly reduces the extent of delocalization; hence, Θ values become considerably more negative.

The T_N values of Rb_xVF_3 are quite explicitly defined by plots of σ vs. T shown in Figure 3. Interestingly, T_N varies with x. This is again related to the changes in magnetic interactions, which involve both ferromagnetic and antiferromagnetic components. Apparently, the decrease in the ferromagnetic component reduces the total ordering energy, resulting in T_N values $\sim$5 K. The magnetically ordered states of both Rb_xVF_3 and Cs_xVF_3 are antiferromagnetic overall. An analysis of the ordering would require a knowledge of the ordered structure, which could only be obtained by neutron diffraction. It is certain that the ordered structure is complex as there exist two constraints to magnetic ordering per V atom. The ordered structure, therefore, is a frustrated one in which magnetic moments are forced antiparallel to directions preferred by some of their nearest-neighbor interactions.

Finally, there appears to be small spontaneous moments associated with the cubic phase in Rb_xVF_3, as in Cs_xVF_3. The moments in Rb_xVF_3 are smaller than those in Cs_xVF_3 and decrease to about 0.02 μ_B at $x = 0.50$, as they did in Cs_xVF_3. At $x = 0.55$, the moment increases again, which is probably a measure of structural defects.

Conclusions. In both Rb_xVF_3 and Cs_xVF_3 systems, the magnetic data support X-ray and optical results and the conclusions regarding V^{2+}–V^{3+} ionic ordering. In the paramagnetic region (above $\sim$30 K), C_M values indicate the orbital moment is partially quenched in the cubic phase but totally quenched in the orthorhombic. The Θ values support the conclusion that delocalization (ferromagnetic contribution) as well as correlation (antiferromagnetic contribution) is involved in the magnetic exchange mechanism. Delocalization is optimized in the cubic phase. In Cs_xVF_3, orthorhombic distortion is small and delocalization is decreased only slightly; but in Rb_xVF_3, the orthorhombic distortion considerably reduces delocalization as seen by the significant change in Θ. The T_N values in Cs_xVF_3 are invariant because atomic positions are not significantly altered by ionic ordering, so correlation and delocalization remain in balance. The Rb_xVF_3 system, however, reflects an imbalance of these effects in its orthorhombic phase as delocalization becomes reduced. At temperatures below T_N small induced magnetic moments are associated with the cubic phase, which further supports the conclusion that V^{2+} and V^{3+} are random in this phase.

Electronic ordering has been found in the pseudohexagonal A_xVF_3 phases,[2a] in the tetragonal K_xVF_3 phase,[2b] and now in the modified pyrochlore A_xVF_3 phases. It appears that electronic ordering in mixed V^{2+}–V^{3+} fluoride systems is the rule rather than the exception.

Acknowledgment. The authors gratefully acknowledge the National Science Foundation (Grants DMR 79-00313, DMR 76-83360, and DMR 74-11970) for financial support, including the purchase of major equipment, and The University of Mississippi for cost sharing. They also thank the NASA Langley Research Center for the loan of an electromagnet and power supply. Appreciation is expressed to The University of Mississippi Computer Center for providing data reduction time.

Registry No. Rb_xVF_3, 63774-72-1; Cs_xVF_3, 63774-59-4.

Supplementary Material Available: Guinier–Hägg X-ray data for the modified pyrochlore $Rb_{0.50}VF_3$ (Table II) and the modified pyrochlore system Cs_xVF_3 (Table III) (7 pages). Ordering information is given on any current masthead page.

Contribution from the Department of Chemistry, University of Florida, Gainesville, Florida 32611

Dynamic Jahn–Teller Effect in a Manganese(III) Complex. Synthesis and Structure of Hexakis(urea)manganese(III) Perchlorate

HOSSEIN AGHABOZORG, GUS J. PALENIK, R. CARL STOUFER,* and J. SUMMERS

Received January 26, 1982

Hexakis(urea)manganese(III) perchlorate, $[Mn(urea)_6](ClO_4)_3$, crystallizes in the space group $R\bar{3}c$ with $a = 18.124$ (4) Å, $c = 14.042$ (3) Å, and 6 molecules/unit cell. The cation has site symmetry $\bar{3}$, which requires the six Mn–O bonds to be equivalent in an apparent violation of the Jahn–Teller theorem. The Mn–O distance of 1.986 (7) Å is virtually identical with the average value found in various distorted high-spin Mn(III) complexes. An analysis of the mean-square displacements and the visible absorption spectral data is in agreement with the existence of a dynamic Jahn–Teller effect in the cation. The Jahn–Teller radius is estimated to be about 0.33 Å, with a stabilization energy of about 36 kJ.

Introduction

Whenever the subject of the Jahn–Teller effect arises, frequent reference is made to high-spin manganese(III).[1,2] The majority of the octahedral complexes of this d^4 ion are high spin with magnetic moments near the spin-only value;

(1) The reference to Jahn–Teller distortion for six-coordinate, high-spin d^4 ions is found in most inorganic texts. Three common texts containing such a reference are cited in ref 2.

(2) (a) Cotton, F. A.; Wilkinson, G. "Advanced Inorganic Chemistry", 4th ed.; Wiley: New York, 1980; p 680. (b) Purcell, K. F.; Kotz, J. C. "Inorganic Chemistry"; Saunders: Philadelphia, 1977; p 553. (c) Huheey, J. E. "Inorganic Chemistry", 2nd ed.; Harper and Row: New York, 1978; p 378.

0020-1669/82/1321-3903$01.25/0